Spin-orbit effects in two-electron emission from ferromagnetic surfaces

F. Giebels,[1] H. Gollisch,[1] and R. Feder[1,2]
[1]*Theoretische Festkörperphysik, Universität Duisburg-Essen, 47048 Duisburg, Germany*
[2]*Max-Planck Institut für Mikrostrukturphysik, Weinberg 2, 06120 Halle, Germany*
(Received 22 August 2013; published 16 October 2013)

In previous experiments on electron-induced two-electron emission from the ferromagnetic surface system Co/W(110), spin-orbit coupling effects have been observed, which are comparable in size to the magnetic exchange effects. The present theoretical work aims at a detailed understanding of such effects, in particular their relation to the spin-dependent electronic structure and to collision dynamics. To this end, we have developed a formalism, which is based on a Dirac equation with an effective magnetic field. Magnetic exchange and spin-orbit coupling are thus incorporated simultaneously. Typical numerical two-electron emission results are presented for W(110) and for ultrathin Co films on W(110) together with the underlying spin- and layer-resolved valence electron spectral density. More detailed insight is provided by calculations, in which SOC was selectively switched off for the valence electron and for the primary and emitted electrons. Our theoretical results are in overall agreement with the experimental data. Furthermore, we predict sizable magnetic dichroism.

DOI: 10.1103/PhysRevB.88.155422 PACS number(s): 73.20.At, 71.70.Ej, 79.60.−i

I. INTRODUCTION

For ferromagnetic crystalline solids and surfaces, spin-orbit coupling (SOC) is of importance in many respects, both from a fundamental and an applicational point of view. It may suffice here to mention just a few of the most prominent SOC effects. Being responsible for magnetocrystalline anisotropy, SOC plays a key role in determining the preferred direction of the magnetization (cf. review article,[1] and references therein). The quasiparticle states and their dispersion relations (band structure, spectral functions) are modified by SOC in ways which give rise to a variety of new phenomena in optical and electron spectroscopies (cf. the monograph[2]). In the latter, the energy- and angle-resolved intensity of electrons, which are emitted from the surface of a ferromagnet, in general depends on the magnetization direction. In particular, its magnitude changes when the magnetization is reversed. This type of phenomenon, which originates from the joint action of spin-orbit coupling and magnetic exchange, is commonly referred to as magnetic dichroism. In its most elementary form, it occurs in spin-polarized low-energy electron diffraction (SPLEED). While for a spin-polarized primary beam SOC and magnetic exchange produce diffracted-beam intensity asymmetries $A_{\rm so}$ and $A_{\rm ex}$, respectively,[3–5] even for an unpolarized primary beam they give rise to an asymmetry A_u upon reversal of the magnetic field.[4,5] Various forms of magnetic dichroism are known in angle-resolved photoemission from valence bands (cf, Ref. 6, and references therein) as well as from core levels (Refs. 7 and 8, and references therein) of solid surface systems. In atomic physics, a very closely related effect, so-called orientational dichroism, has been observed in the ionization of polarized atoms by electron impact[9] and by ion impact.[10]

The present work deals with two-electron emission from ferromagnetic surfaces following the collision of a primary low-energy electron with a valence electron. For short referred to as $(e,2e)$, this coincidence spectroscopy has a long history of intense experimental and theoretical study in atomic physics (cf., e.g., Refs. 11–13, and ample references therein). In solid state physics, $(e,2e)$ has over the past two decades evolved into a very powerful tool for studying collision dynamics, pair diffraction, correlation effects, and electronic structure at solid surfaces (cf. Refs. 14–18, and ample references therein).

Since the $(e,2e)$ reaction cross section comprises matrix elements between the valence state, primary, and outgoing electron states and since SOC has a considerable influence (increasing with increasing atomic number Z) on all these four one-electron states, it can be expected to be of importance for $(e,2e)$. For nonmagnetic surfaces, this was first demonstrated by numerical calculations for the large-Z surface W(001)[19] and subsequently confirmed by experiment.[20,21] For ferromagnetic surfaces appreciable SOC effects have been found experimentally for an ultrathin Co film on W(110).[22–24] While SOC is fairly weak for Co ($Z = 27$), the substrate W(110) with its large $Z = 74$ affects the electronic states of the combined system such that the SOC-induced intensity asymmetry $A_{\rm so}$ upon reversal of the spin of the primary electrons reaches about the same size as its exchange-induced counterpart $A_{\rm ex}$.

On the theoretical side, SOC could so far be included in $(e,2e)$ calculations only for nonmagnetic surfaces, whereas for ferromagnets it had to be neglected. This can in good approximation be acceptable for low-Z systems like clean Fe and Co surfaces. For ferromagnetic surface systems like $3d$ ferromagnet films on a W substrate, which involve a large-Z material, it is however mandatory to include SOC in $(e,2e)$ calculations. In this paper, we present an $(e,2e)$ formalism, in which the four ingredient one-electron states are solutions of a Dirac equation with an effective magnetic field. Ferromagnetism and SOC are thereby treated simultaneously on an equal footing. With this formalism implemented in a rather complex computer code, we performed numerical calculations for Co an W(110) and for clean W(110). The real part of the quasiparticle potential input for these calculations was obtained by density functional theory *ab initio* calculations of the ground state, which also yielded the magnetic moments in the individual atomic layers parallel to the surface.

As numerical results, we present and discuss fully spin-resolved cross sections (intensities) and spin asymmetries derived from them. Calculated spectra of the SOC- and magnetism-induced asymmetries $A_{\rm so}$ and $A_{\rm ex}$ are in overall

agreement with their experimental counterparts.[22] While these two asymmetries can only be obtained using a spin-polarized primary beam, we predict a sizable third asymmetry A_u, which is produced already by an unpolarized primary beam upon reversal of the magnetization, i.e., magnetic dichroism.

Wishing to gain more insight into the underlying physical mechanisms, one has to bear in mind that experimentally observed intensities and asymmetries are affected jointly by SOC in the valence electron state, the primary electron state, and the outgoing electron states. In experimental reality, SOC always acts in all four states. In theory, however, SOC can be switched off selectively in the individual states. Comparison of such "switch-off" spectra with the ones with SOC in all states makes it possible to identify the origin of specific features in the spectra as mainly due to SOC in the valence electron states or the primary and emitted electron states.

This paper is organized as follows. In Sec. II we present a relativistic theory of $(e,2e)$ from crystalline ferromagnets. Section III deals with symmetry-induced properties of spin-dependent $(e,2e)$ reaction cross sections for magnetic cubic (110) surface systems. Section IV is devoted to $(e,2e)$ from W(110) and ultrathin magnetic Co films on W(110): after specifying essential model features and input for calculations, numerical results are presented and discussed. A summary and an outlook are given in Sec. V.

II. THEORETICAL FRAMEWORK

The $(e,2e)$ setup, which we employ in the present work, is sketched in Fig. 1. A primary electron impinges on the surface of a crystalline collinear ferromagnet, collides with a valence electron, and the two electrons exit from the solid and are then detected in coincidence.

Including many-body effects via optical potentials, this process is governed by a two-electron Hamiltonian of the form

$$H = H_1 + H_2 + U. \tag{1}$$

H_1 and H_2 are one-electron Hamiltonians, which incorporate the interaction of each of the two electrons with the crystal,

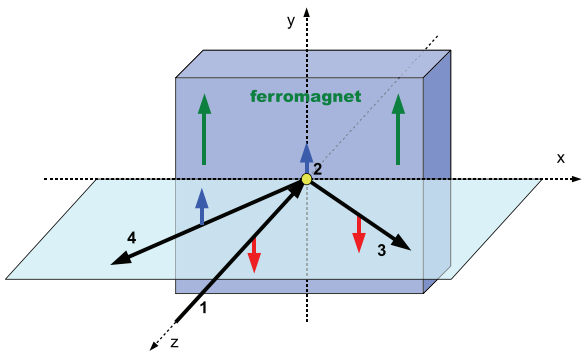

FIG. 1. (Color online) Sketch of the $(e,2e)$ setup used in the present work. The numbers 1 to 4 indicate the four ingredient one-electron states $|i\rangle$ with energies E_i, surface-parallel momenta $\vec{k}_i^{\parallel}$, and spin labels $\sigma_i = \pm$ (for spin quantization axis y). After the collision of a primary electron (state $|1\rangle$) with a valence electron (state $|2\rangle$), two electrons (correlated states $|3\rangle$ and $|4\rangle$) are emitted and detected. The two long vertical arrows symbolize the majority spins of the ferromagnetic crystal aligned in the $+y$ direction.

and U is a two-body potential which represents the interaction between the two electrons. If both electrons are in the vacuum region between the surface and the detectors, U is the bare Coulomb interaction. If at least one electron is inside the crystal, U is a screened Coulomb potential.

For each of the two one-electron Hamiltonians H_i (with $i = 1,2$) in Eq. (1) we use a Dirac Hamiltonian with an electrostatic potential V and a magnetic field $\vec{B}$

$$H_i = c\vec{\alpha}\cdot\vec{p} + mc^2\beta + V + \mu_B\beta\,\vec{\Sigma}\cdot\vec{B}, \tag{2}$$

where $\vec{\alpha} = (\alpha_1,\alpha_2,\alpha_3)^T$ and β are the usual 4×4 Dirac matrices, $\vec{\Sigma} = (\Sigma_1,\Sigma_2,\Sigma_3)^T$ are the 4×4 Pauli spin matrices, and μ_B is the Bohr magneton (cf. standard textbooks on quantum mechanics). H_i has the same form as the Dirac-Kohn-Sham Hamiltonian in relativistic spin density functional theory (neglecting the creation of particle-antiparticle pairs and the coupling between $\vec{B}$ and the orbital current) (cf. the recent comprehensive monograph[25] and ample references therein). In the present $(e,2e)$ context, however, V and $\vec{B}$ do not pertain to the ground state, but to excited quasiparticle states, i.e., they are optical potentials which have imaginary parts.

Spin-orbit coupling (SOC), which is inherent in the first three terms of Eq. (2), and ferromagnetic exchange coupling, which is represented by the last term, are treated on an equal footing. Nonmagnetic systems are described by Eq. (2) with $\vec{B} = 0$.

Since we are dealing with collinear ferromagnetism, the direction of $\vec{B}$ is uniform throughout the crystal. Some more physical insight as well as computational advantage can then be gained by transforming to a coordinate system such that $\vec{B} = (0,0,B)^T$. The last term in Eq. (2) then becomes $\mu_B B\beta\Sigma_3$ and one can combine it with the potential matrix $V\cdot 1_4$ to a new potential matrix, which has only the diagonal elements (V^+,V^-,V^-,V^+) with $V^\pm = V\pm\mu_B B$. Focusing on the upper two (large) components of the Dirac four-spinors, V^+ is seen to act only on the spin-up component and V^- only on the spin-down component.

For the calculation of the quasiparticle eigenstates of the one-electron Hamiltonian [Eq. (2)] we use a layer-KKR method, which has first been developed for the scattering states in spin-polarized low-energy electron diffraction (SPLEED) (cf. Ref. 5, and references therein) and later on, in a Green function version, for the valence electron states required in photoemission calculations.[26]

For the calculation of the $(e,2e)$ reaction cross section we adapted a formalism, which has previously been presented in detail.[14,27] Its central ingredient is a Coulomb interaction matrix element

$$\langle 3,4|U|1,2\rangle \tag{3}$$

between a two-quasiparticle initial state $|1,2\rangle$ which represents the incident electron and a valence electron of the solid, and a two-quasiparticle final state $|3,4\rangle$ which embodies the two outgoing electrons. As explained in Ref. 27, this matrix element is not a first Born approximation but equivalent to the (exact) T-matrix element if $|1,2\rangle$ is an eigenstate of $H_1 + H_2$ and the final state $|3,4\rangle$ is one of the complete two-electron Hamiltonian H [cf. Eq. (1)], i.e., including the electron-electron interaction U.

Both two-electron states have as basic ingredients one-electron states $|i\rangle$ (with $i = 1,2,3,4$), which are eigenstates of the Dirac Hamiltonian Eq. (2). These states have sharp kinetic energies E_i and surface-parallel momenta $\vec{k}_i^{\parallel}$. Due to spin-orbit coupling, they are of course not eigenstates of a chosen spin operator component. They may however still be characterized by a spin label σ_i, which in the case of the incident and outgoing electrons corresponds to the definite spin orientation at the electron source and at the detectors, respectively. As is obvious from Eq. (2), these one-electron states depend on the direction and magnitude of the magnetic field $\vec{B}$.

The two-electron initial state $|1,2\rangle$ is then an antisymmetrized product of the projectile electron state $|1\rangle$, which is a LEED state with energy E_1, surface-parallel momentum $\vec{k}_1^{\parallel}$ and spin σ_1 asymptotically at the electron gun, and a valence electron state $|2\rangle$ with energy E_2, surface-parallel momentum $\vec{k}_2^{\parallel}$, and spin label σ_2. The U-correlated final state $|3,4\rangle$ has the form

$$|3,4\rangle = (1/\sqrt{2})(|3\rangle|4\rangle F_{\rm corr} - |4\rangle|3\rangle F_{\rm corr}^*). \tag{4}$$

The two one-electron states $|3\rangle$ and $|4\rangle$ are time-reversed LEED states with asymptotic boundary conditions such that an electron with momentum $\vec{k}_3$ and spin orientation σ_3 (with respect to a given axis) arrives at one detector and an electron with momentum $\vec{k}_4$ and spin σ_4 at the other detector. The correlation factor $F_{\rm corr}$ embodies the Coulomb interaction and is actually a function of the coordinates of the two electrons, which depends on their relative momentum.

Substituting Eq. (4) into Eq. (3) yields direct matrix elements

$$f_{\sigma_3\sigma_4}^{\sigma_1\sigma_2\mu} = \langle 3|\langle 4|F_{\rm corr}^* U|1\rangle|2\rangle \tag{5}$$

and exchange matrix elements

$$g_{\sigma_3\sigma_4}^{\sigma_1\sigma_2\mu} = \langle 4|\langle 3|F_{\rm corr} U|1\rangle|2\rangle. \tag{6}$$

In the above, the index $\mu = +$ ($\mu = -$) indicates that the magnetic field $\vec{B}$ is antiparallel (parallel) to a specified unit vector $\vec{e}$ (e.g., the Cartesian unit vector $\vec{y}$ as in Fig. 1), i.e., the majority spin direction of the ferromagnet is parallel (antiparallel) to $\vec{e}$.

The $(e,2e)$ reaction cross section, referred to in the following as "intensity", is then

$$I_{\sigma_3\sigma_4}^{\sigma_1\mu} = \frac{k_3 k_4}{k_1} \sum_{E_2,\vec{k}_2^{\parallel},\sigma_2} \left| f_{\sigma_3\sigma_4}^{\sigma_1\sigma_2\mu} - g_{\sigma_3\sigma_4}^{\sigma_1\sigma_2\mu} \right|^2 \delta, \tag{7}$$

where $k_i = \sqrt{2E_i}$ and δ stands for the conservation of energy

$$E_1 + E_2 = E_3 + E_4 \tag{8}$$

and of surface-parallel momentum

$$\vec{k}_1^{\parallel} + \vec{k}_2^{\parallel} = \vec{k}_3^{\parallel} + \vec{k}_4^{\parallel} + \vec{g}^{\parallel}, \tag{9}$$

where $\vec{g}$ is a surface-parallel reciprocal lattice vector. For each majority spin orientation ($\mu = \pm$), there are thus eight spin-dependent $(e,2e)$ intensities $I_{\sigma_3\sigma_4}^{\sigma_1\mu}$. Generally, they are all nonzero and different from each other. In particular, there are, as a consequence of SOC, "spin-flip" intensities like $I_{-,-}^{+,\mu}$, i.e., the primary electron has spin up and both ejected electrons have spin down.

Since the resolution of the outgoing electron spins σ_3 and σ_4 is—to our knowledge—not yet feasible experimentally, the currently observable $(e,2e)$ intensities involve sums over the outgoing electron spins:

$$I^{\sigma_1\mu} := \sum_{\sigma_3,\sigma_4} I_{\sigma_3\sigma_4}^{\sigma_1\mu}. \tag{10}$$

In formal analogy to what was found to be useful in SPLEED (cf. Ref. 5, and references therein), these four intensities can be transformed into an intensity sum

$$I = \sum_{\sigma_1\mu} I^{\sigma_1\mu} \tag{11a}$$

and three asymmetries,

$$A_{\rm so} = [(I^{++} + I^{+-}) - (I^{-+} + I^{--})]/I, \tag{11b}$$

$$A_{\rm ex} = [(I^{++} + I^{--}) - (I^{+-} + I^{-+})]/I, \tag{11c}$$

$$A_u = [(I^{++} + I^{-+}) - (I^{+-} + I^{--})]/I. \tag{11d}$$

In the limit of vanishing SOC the intensities $I^{\sigma_1\mu}$ depend only on the alignment of the primary spin relative to the magnetic field $\vec{B}$, i.e., $I^{\sigma_1\mu} = I^{-\sigma_1,-\mu}$. From Eqs. (11b) and (11d) it is then evident that $A_{\rm so}$ and A_u are zero. If the magnetic field $\vec{B}$ goes to zero (i.e., no ferromagnetism), $I^{\sigma_1\mu} = I^{\sigma_1,-\mu}$ and consequently $A_{\rm ex} = 0$ and $A_u = 0$. SOC is necessary and sufficient for nonvanishing $A_{\rm so}$, as is ferromagnetism ("magnetic exchange") for $A_{\rm ex}$, hence the subscripts "so" and "ex". Quantitatively, $A_{\rm so}$ is however influenced by magnetism and so is $A_{\rm ex}$ by SOC.

A_u requires for its existence both SOC and magnetism. Since the sum of two oppositely polarized primary beams ($\sigma_1 = \pm$) corresponds to an unpolarized beam, the sum of the first (last) two intensities in Eq. (11d) is the intensity due to an unpolarized primary beam for majority spin orientation $\mu = +$ ($\mu = -$). This means that the asymmetry A_u can be obtained using an unpolarized primary electron beam (hence the subscript "u") and reversing the magnetic field. It thus represents a form of magnetic dichroism and may be termed "dichroic asymmetry".

III. SYMMETRY PROPERTIES FOR CUBIC(110) SURFACES

In order to explore the interplay of ferromagnetism and SOC in $(e,2e)$ spectroscopy, it is desirable to have a surface system with strong SOC. Clean surfaces of $3d$ ferromagnets are not so suitable, since SOC is rather weak due to their low Z. For ultrathin magnetic films on a large-Z substrate, however, sizable SOC effects are possible, as has been demonstrated in experimental $(e,2e)$ work for the case of Co on W(110).[22,23] We have therefore chosen this surface system for the first application of our $(e,2e)$ theory. Prior to presenting numerical results (in Sec. IV), we focus on some general properties of spin-resolved $(e,2e)$ intensities, which are dictated by symmetry for ferromagnetic cubic(110) surfaces.

We first recall that the point group $2mm$ for a nonmagnetic cubic(110) surface has four symmetry operations: the identity, a twofold rotation about the surface normal, the reflection m_y

at the (x,z) plane, and the reflection m_x at the (y,z) plane. The single group has the four one-dimensional irreducible representations $\Sigma^i, i = 1,\ldots,4$, and the double group (in the presence of SOC) has the single two-dimensional irreducible representation Σ_5. If the surface is ferromagnetic with magnetization along y, the symmetry is reduced to the point group m, with the two symmetry operations identity and m_y. Its double group has two one-dimensional irreducible representations, γ_+ and γ_-, which are degenerate by time reversal (cf., e.g., Ref. 28, and references therein).

As the $(e,2e)$ geometry we choose—like in the experiment by Samarin *et al.*[22,23]—a coplanar setup as shown in Fig. 1. The coordinate system is such that z is along the (outward-directed) surface normal [110], and x and y are in the surface plane along [001] and [1 −1 0], respectively. The primary electrons are incident along the surface normal and the electron pairs are emitted in the (x,z) plane at polar angles ϑ_3 and ϑ_4 and azimuthal angles $\varphi_3 = 0^\circ$ and $\varphi_4 = 180^\circ$. The parallel momenta of the two outgoing electrons thus have only x components $k_{3x} = \sqrt{2E_3}\sin\vartheta_3$ and $k_{4x} = -\sqrt{2E_4}\sin\vartheta_4$. The spin-dependent $(e,2e)$ intensities are then functions of the primary electron energy E_1, the energies E_3 and E_4 of the outgoing electrons, and of their parallel-momentum components k_{3x} and k_{4x}.

The primary electron spin polarization $\vec{P}_1$ is chosen normal to the reaction plane, i.e., along $\pm y$, and is characterized by the spin label $\sigma_1 = \pm$. The effective magnetic field $\vec{B}$ in Eq. (2) is along $\mp y$, i.e., the majority (minority) spin orientation is $\pm y$ ($\mp y$), with corresponding "magnetism label" $\mu = \pm$. Since the entire initial setup, including the primary polarization vector $\vec{P}_1$, is invariant under the mirror operation m_y, the polarization vectors $\vec{P}_3$ and $\vec{P}_4$ of the two emitted electrons can have only components along $\pm y$. Consequently, they can be completely characterized by the spin labels $\sigma_3 = \pm$ and $\sigma_4 = \pm$.

We now turn to the symmetry properties of the spin-dependent $(e,2e)$ intensities [cf. Eqs. (7) and (10)] and the asymmetries associated with them [cf. Eqs. (11b)–(11d)], which in our setup are all, as explained above, functions of the primary electron energy E_1, the energies E_3 and E_4 of the outgoing electrons, and of their parallel-momentum components k_{3x} and k_{4x}.

First consider the fully spin-resolved intensities $I^{\sigma_1\mu}_{\sigma_3\sigma_4}$ [cf. Eq. (7)]. The mirror operation m_x, which is a symmetry operation of the system without ferromagnetism, reverses the primary electron spin and the magnetization. Since in the present setup the primary electron momentum is normal to the surface, it is not affected by m_x. As for the outgoing electrons, m_x interchanges the energies E_3 and E_4, and interchanges and reverses the parallel momentum components k_{3x} and k_{4x} as well as the spin labels σ_3 and σ_4. Therefore, for fixed primary energy E_1, we have

$$I^{\sigma_1\mu}_{\sigma_3\sigma_4}(E_3,k_{3x};E_4,k_{4x}) = I^{-\sigma_1,-\mu}_{-\sigma_4,-\sigma_3}(E_4,-k_{4x};E_3,-k_{3x}). \quad (12)$$

For the spin-summed intensities $I^{\sigma_1\mu}$ [cf. Eq. (10)] this implies

$$I^{\sigma_1\mu}(E_3,k_{3x};E_4,k_{4x}) = I^{-\sigma_1,-\mu}(E_4,-k_{4x};E_3,-k_{3x}). \quad (13)$$

From this relation one obtains immediately the following properties of the asymmetries [cf. Eqs. (11b)–(11d)]:

$$A_{\rm ex}(E_3,k_{3x};E_4,k_{4x}) = A_{\rm ex}(E_4,-k_{4x};E_3,-k_{3x}), \quad (14a)$$
$$A_{\rm so}(E_3,k_{3x};E_4,k_{4x}) = -A_{\rm so}(E_4,-k_{4x};E_3,-k_{3x}), \quad (14b)$$
$$A_u(E_3,k_{3x};E_4,k_{4x}) = -A_u(E_4,-k_{4x};E_3,-k_{3x}). \quad (14c)$$

If the polar angles ϑ_3 and ϑ_4 are fixed, k_{3x} and k_{4x} are functions only of E_3 and E_4, and so are then all the above $(e,2e)$ quantities. Since from energy and parallel-momentum conservation [cf. Eqs. (8) and (9)] it follows that a pair (E_3, E_4) corresponds uniquely to a pair (E_2, k_{2x}), the $(e,2e)$ quantities can alternatively be represented as functions of the energy E_2 and the parallel-momentum component k_{2x} of the relevant valence electron. Since the mirror operation at the (y,z) plane transforms k_{2x} into $-k_{2x}$, we obtain for the intensities the symmetry relations

$$I^{\sigma_1\mu}_{\sigma_3\sigma_4}(E_2,k_{2x}) = I^{-\sigma_1,-\mu}_{-\sigma_4,-\sigma_3}(E_2,-k_{2x}), \quad (15)$$

$$I^{\sigma_1\mu}(E_2,k_{2x}) = I^{-\sigma_1,-\mu}(E_2,-k_{2x}). \quad (16)$$

For the asymmetries [cf. Eqs. (11b)–(11d) and (14)], Eq. (16) entails

$$A_{\rm ex}(E_2,k_{2x}) = A_{\rm ex}(E_2,-k_{2x}), \quad (17a)$$
$$A_{\rm so}(E_2,k_{2x}) = -A_{\rm so}(E_2,-k_{2x}), \quad (17b)$$
$$A_u(E_2,k_{2x}) = -A_u(E_2,-k_{2x}). \quad (17c)$$

For the spin- and layer-resolved valence electron density of states (LDOS alias spectral density) $N^{\sigma_2\mu}_m(E_2,k_{2x})$, where m indicates the atomic layer parallel to the surface and $\sigma_2 = \pm$ the valence electron spin with respect to the $+y$ direction, symmetry imposes a relation analogous to Eq. (16):

$$N^{\sigma_2\mu}_m(E_2,k_{2x}) = N^{-\sigma_2,-\mu}_m(E_2,-k_{2x}). \quad (18)$$

An important special case is the equality of the two emission angles: $\vartheta_3 = \vartheta_4$. If in this case the two energies E_3 and E_4 are equal, $k_{3x} = -k_{4x}$ and consequently $k_{2x} = 0$ (i.e., center of the surface Brillouin zone). The above $(e,2e)$ quantities and the LDOS are then functions of only the valence energy E_2. $A_{\rm so}$ and A_u are identically zero, whereas $A_{\rm ex}$ in general has some finite value.

All the above relations remain of course valid for nonmagnetic materials, with the simplification that the magnetic index μ is absent and $A_{\rm ex} = A_u = 0$.

IV. COBALT FILMS ON W(110)

As a typical ferromagnetic surface system, for which spin-orbit coupling is important, we chose magnetic few-monolayer Co films on W(110) since for this system experimental $(e,2e)$ data are available[22] for comparison with our theoretical results. We also included the clean W(110) in the present study. In the following, we first specify the essential model ingredients used in our calculations and then present spin-resolved $(e,2e)$ results together with the associated valence electron densities of states.

A. Model specifications

In this section we deal with three essential prerequisites for our $(e,2e)$ calculations: the surface geometry, the electronic structure of the ground state, and the complex quasiparticle potentials appropriate for $(e,2e)$.

We first address the surface geometry. For the clean W(110) surface, LEED[29–31] and surface x-ray diffraction[32] studies have shown that it is unreconstructed except for a contraction of the first interlayer spacing by about 3% relative to the bulk interlayer spacing. The epitaxial growth of Co films on W(110), however, is rather complicated (cf., e.g., Refs. 33–35). Initial growth is pseudomorphic. But before a pseudomorphic adlayer is complete, areas with hexagonally close packing are formed. Further Co deposition (at room temperature) leads to a structural change from pseudomorphic to hexagonally close-packed (hcp) and to a layer-by-layer growth of subsequent hcp monolayers. For $n > 2$ monolayers one thus obtains a strained hcp Co n-monolayer film, which is incommensurate with the W(110) substrate or has only a very large surface-parallel unit cell in common with it. Such structure is not tractable in the computer code (FLAPW/FLEUR[36]), which we use for the calculation of the electronic structure of the ground state, nor in our $(e,2e)$ code. Moreover, the above complicated growth would obscure the basic evolution of spin-orbit and ferromagnetic exchange effects in $(e,2e)$ with an increasing number of adsorbed monolayers, which we want to explore in the present pilot study.

We therefore adopt the simpler geometrical model of a pseudomorphic layer-by-layer growth of Co on W(110). The Co films of one and two monolayers, which we intend to focus on, are thus commensurate with the W substrate, i.e., the lateral positions of the Co atoms are fixed.

The interlayer distances $d_{\text{Co-Co}}$ and $d_{\text{Co-W}}$, which are needed as an initial input for our ground state calculations, are chosen as follows. In the Co layers and in the topmost W layer, we assume the maximal nonoverlapping muffin tin spheres of bulk hcp Co (with radius $r_{mt} = 2.362$ Bohr) and of bulk W (with radius $r_{mt} = 2.590$ Bohr), respectively. The interlayer distances are then determined such that the muffin tin spheres in adjacent layers touch but do not overlap each other. This yields $d_{\text{Co-Co}} = 3.657$ and $d_{\text{Co-W}} = 3.947$ Bohr, i.e., a reduction of 13.5% and 6.6% relative to the bulk W interlayer spacing $d_{\text{W-W}} = 4.226$ Bohr. The spacing between the two topmost W layers is assumed to be the same as in the W bulk, since the 3% inward relaxation of the topmost layer of clean W(110) is likely to be lifted by the adsorption of Co.

Since the maximal muffin-tin radii of bulk hcp Co are quite close to those of bulk bcc Fe, it is not uninteresting to compare the above interlayer distance values with those obtained by total energy minimization calculations for Fe films on W(110) (Refs. 37 and 38, and references therein), which actually grow pseudomorphically. For example, $d_{\text{Fe-Fe}} = 3.65$ Bohr according to Ref. 38, which is almost the same as our above $d_{\text{Co-Co}}$, and $d_{\text{Fe-Fe}} = 3.34$ Bohr according to Ref. 37. In summary, the interlayer distance values of our simple touching-spheres model for Co/W(110) are well within the range of values obtained by more sophisticated methods for Fe/(W(110).

For clean W(110) and for one and two monolayers Co on W(110) (with the above surface geometry) we calculated the electronic structure of the ground state by means of an *ab initio* full-potential linear augmented-plane-wave (FLAPW) method[36] with a local density approximation for the exchange-correlation energy.[39] The films needed in this method were chosen to consist of 11 monolayers in the case of clean W(110). For the n-monolayer Co systems they were composed of $(11 + 2n)$ monolayers, i.e., the 11-layer W film augmented on each side by n Co layers.

TABLE I. Spin magnetic moments in the Co layers and adjacent two W layers of pseudomorphic films of 1 ML and 2 ML Co on W(110).

	1 ML Co/W m (μ_B)	2 ML Co/W m (μ_B)
Co (2)		2.017
Co (1)	1.606	1.578
W (1)	0.023	−0.004
W (2)	−0.003	−0.006

The spin magnetic moments obtained in these ground state calculations are given in Table I. In the Co layer adjacent to the topmost W layer, the magnetic moments are slightly less than the magnetic moment of bulk hcp Co (1.62 μ_B), whereas in the topmost Co layer of the 2 ML film they are enhanced by about 23%. In the W layers they are extremely small, much less than the -0.1 μ_B found for ultrathin Fe films on W(110).[37,38]

The real potentials obtained in the above ground state calculations were augmented by a spatially uniform energy-dependent complex self-energy correction and an image-asymptotic tail of the surface potential barrier to yield quasiparticle potentials appropriate for electrons involved in the $(e,2e)$ process.

In particular, the imaginary part V_{im} of the self-energy, which accounts for electron and hole lifetimes, was chosen as follows. For the W layers, V_{im} for the incoming and outgoing electron states, which are LEED states and time-reversed LEED states, respectively, was taken as $V_{im} = -0.1(E + \phi)^{0.83}$, where E is the kinetic energy (relative to the vacuum level) and $\phi = 5.07$ eV the work function of W(110). LEED spectra calculated using this V_{im} were found to agree well with experiment in Refs. 40–42 for the W valence electrons we used, guided by peak widths in photoemission experimental data.[43,44]

The imaginary self-energy part for the valence electron states in the Co layers was adopted from experimental photoemission data.[45] For the LEED-type states we used a form guided by spin-dependent mean free path experimental data.[46–48] These forms of $V_{im}(E)$ are appreciably spin dependent. For the valence electrons, V_{im} is stronger for majority spin than for the minority spin, whereas for the LEED-type electrons it is the other way round.

To assess the relevance of our above model characteristics for real Co films on W(110), we calculated specular beam LEED spectra (at normal incidence) and compared them to experimental data.[42] They are in very good agreement for clean W(110), as already mentioned above, and also for 1 ML Co on W(110). For 2 ML Co, the agreement between experiment[42] and theory became rather good by using a somewhat larger

value $d_{\text{Co-Co}}$ (reduced relative to $d_{\text{W-W}}$ by 10.9% instead of the above 13.5%). We therefore employed this value in our $(e,2e)$ calculations. As far as LEED is concerned, our pseudomorphic growth model thus appears to mimick fairly well the actual structure of the Co films.

B. Electron pair emission results

In the following, we present typical $(e,2e)$ results for clean W(110) and for one and two ferromagnetic monolayers of Co on W(110) in conjunction with the underlying spin- and layer-resolved valence electron densities of states (LDOS). Our calculations were done for the coplanar geometrical setup, which has been shown in Fig. 1 and explained in more detail in the third and fourth paragraph of Sec. III. In particular, the reaction plane is the (x,z) plane (with z along the surface normal [110] and x in the surface plane along [001]), the primary electron with fixed energy E_1 is incident normal to the surface and the two electrons are emitted in the (x,z) plane at fixed polar angles ϑ_3 and ϑ_4. As deduced in Sec. III, the $(e,2e)$ intensities can then be represented as functions of the valence electron energy E_2 and parallel momentum component k_{2x}, i.e., $I^{\sigma_1\mu}_{\sigma_3\sigma_4}(E_2,k_{2x})$. This representation has the advantage of directly revealing the relationship between $(e,2e)$ spectra and the associated valence electron LDOS $N^{\sigma_2}_m(E_2,k_{2x})$.

The $(e,2e)$ spectra $I^{\sigma_1\mu}_{\sigma_3\sigma_4}(E_2,k_{2x})$ comprise two special cases of particular interest: (a) $k_{2x}=0$ (i.e., center of the surface Brillouin zone), which for equal emission angles $\vartheta_3=\vartheta_4$ corresponds to equal outgoing energies $E_3=E_4$ and (b) $E_2=\text{const}$, which according to Eq. (8)—with E_1 fixed—corresponds to a constant sum energy E_3+E_4.

In view of exploring the relation between the valence electron structure and the pair emission spectra, it is important to recall two $(e,2e)$ selection rules,[49] which hold for our above-specified geometry. Since our reaction plane (x,z) is a mirror plane of the semi-infinite surface system, only valence states with even mirror symmetry are allowed to contribute. This is strictly valid in the absence of spin-orbit coupling (SOC). With SOC, the valence electron spinor generally contains both even and odd spatial parts, but its even spatial part is the most relevant one for $(e,2e)$. The odd part may contribute, because due to SOC the incident and outgoing electron spinors have also odd parts (inside the crystal). Since these are much smaller than their even parts, $(e,2e)$ contributions involving odd valence electron parts are generally also much smaller.

For the special case of equal-energy distributions, for which the valence electron parallel momentum is zero, there is a further selection rule (cf. Ref. 49). Only valence states with spatial parts of (single-group) symmetry types Σ_1 and Σ_3 are relevant: both types can contribute to antiparallel spin intensities, whereas parallel-spin intensities can only originate from Σ_3.

In our $(e,2e)$ calculations we chose the polar emission angles $\vartheta_3=\vartheta_4=50^\circ$ and the primary energy $E_1=27$ eV, since for these values experimental $(e,2e)$ data are available[22] for comparison. We first present results for the case of valence electron momentum $\vec{k}_2^{\,\parallel}=0$ (center of the surface Brillouin zone). In Fig. 2(A) we show for clean W(110) $(e,2e)$ spectra $I^{\sigma_1}_{\sigma_3\sigma_4}(E_2)$ together with the underlying valence electron layer-resolved densities of states (LDOS) $N^{\sigma_2}_m(E_2)$ of the single group symmetry types Σ_1 and Σ_3. Since $\vec{k}_2^{\,\parallel}=0$ it suffices to show the results for valence electron spin up (parallel to the y direction in the surface plane), because for spin down the LDOS results are the same, and so are the $(e,2e)$ intensities with all spin labels reversed. In order to identify and analyze spin-orbit effects, we performed calculations including SOC (i.e., fully relativistic) and neglecting SOC (i.e., scalar relativistic).

Let us first consider the LDOS calculated without SOC [Fig. 2(A), panels (f) and (g)]. The bulk LDOS reflects the bulk band structure along the surface normal, with a Σ_1 band below -1.15 eV and a Σ_3 band above. The first and second layer LDOS reveals a surface state of purely Σ_1 symmetry at -1.12 eV, which is split off from the Σ_1 bulk band edge at -1.15 eV. This surface state owes its existence to the 3% inward relaxation of the topmost layer.

SOC induces a gap between bulk bands of Σ_5 symmetry (i.e., with both Σ_1 and Σ_3 spatial parts), as can be seen in Fig. 2(A), panels (a) and (b), from the bulk layer LDOS (labeled Wb). Inside this gap, the first- and second-layer LDOS exhibit the SOC-modified surface state S, which now has, in addition to the Σ_1 part, a substantial Σ_3 contribution. Without the inward relaxation of the surface layer, it would still exist, but be shifted by about 0.05 eV towards lower energy. We note in passing that with finite small parallel momentum this surface state disperses almost linearly and is strongly spin-polarized (cf. Refs. 18, 44, 50, and 51).

The corresponding spin-resolved $(e,2e)$ spectra as functions of valence energy E_2 are presented in panels (c), (d), and (e) of Fig. 2(A). With SOC switched off in all four electron states [Fig. 2(A), panel (e)], the prominent Σ_1 surface state S strongly appears in the antiparallel-spin intensities I^-_{-+} and I^-_{+-}, but is completely absent in the parallel-spin spectrum I^+_{++}, which is in line with the above-quoted $(e,2e)$ selection rules. If SOC is switched on only in the valence state [Fig. 2(A), panel (d)], S manifests itself—due its presence in the Σ_3 LDOS [Fig. 2(A), panel (a)]—also in I^+_{++}. With SOC in all states [Fig. 2(A), panel (c)], there is, in addition to the presence of S in I^+_{++}, a strong splitting between the antiparallel-spin intensities I^-_{-+} (direct process) and I^-_{+-} (exchange process). This splitting, marked by the green (gray) area, reflects mainly the SOC-induced left-right asymmetry in the two outgoing electron states.

Next we present in Fig. 2(B) analogous results for the ferromagnetic system 1 ML Co on W(110). The bottom panels show the valence electron LDOS at the center of the surface Brillouin zone, calculated without SOC. For spatial symmetry Σ_3 [Fig. 2(B), panels (f) and (m)], the Co layer has two broad LDOS peaks, one with spin up around -1.5 eV and one with spin down around -0.7 eV. Since above about -1 eV, Σ_3 orbitals of W are available for hybridization, a pronounced spin-down peak is also found in each of the two topmost W layers. For symmetry Σ_1, the Co spin-up LDOS [Fig. 2(B), panel (g)] is similar to the one for Σ_3, with an additional peak around -0.8 eV, which extends into the adjacent W layers. This peak as well as the peak at -0.6 eV in the Σ_1 spin-down LDOS are due to interference with backward diffraction from the W substrate. If the W substrate is replaced by a refracting but nonreflecting surface barrier, these two peaks are absent,

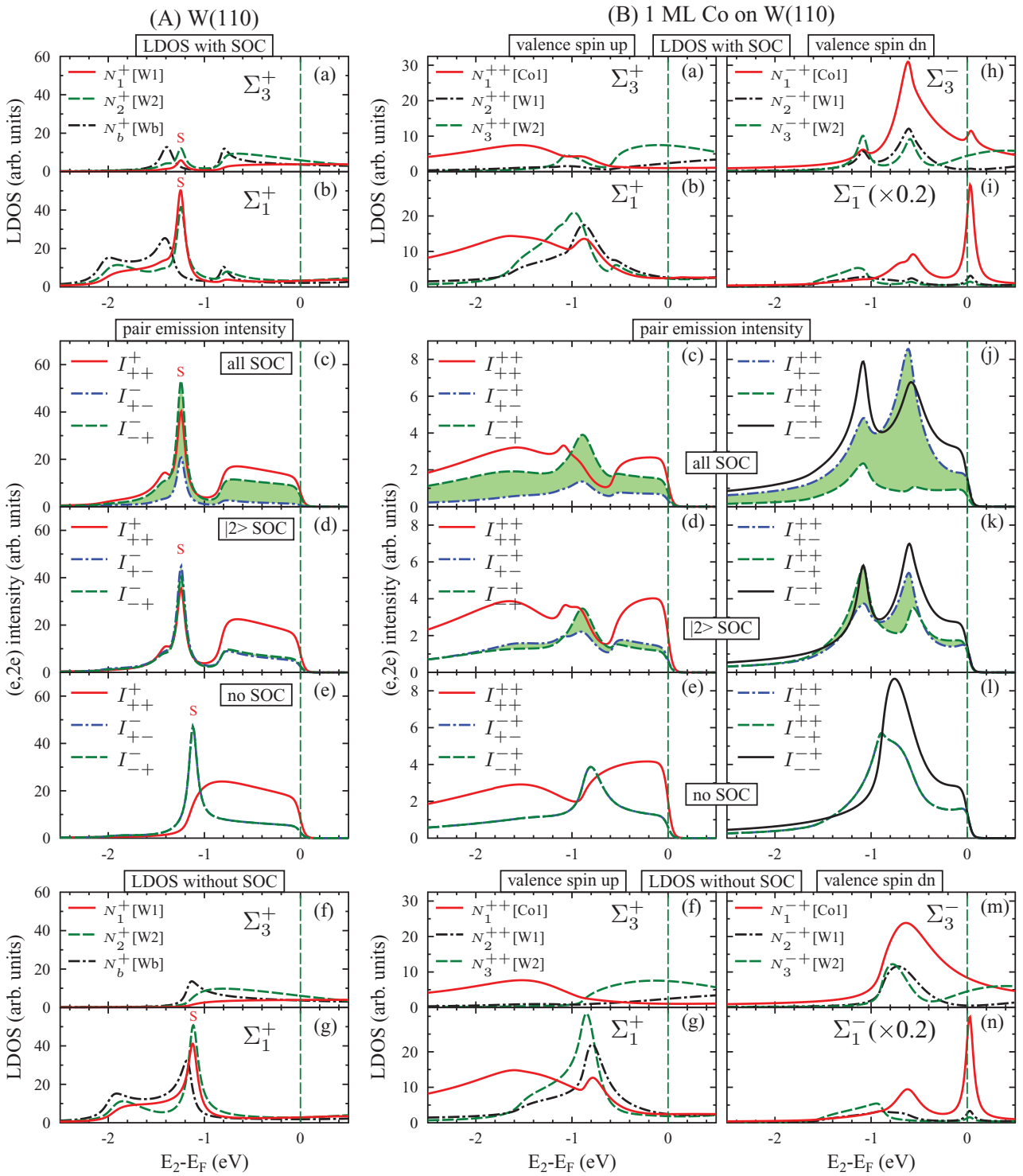

FIG. 2. (Color online) Spin- and layer-resolved valence electron densities of states (LDOS) of spatial symmetry types Σ_1 and Σ_3 for $\vec{k}_2^{\parallel} = 0$ and spin-resolved $(e,2e)$ intensities as functions of the valence electron energy E_2. Primary electrons with energy $E_1 = 27$ eV and spin $\sigma_1 = \pm$ are incident along the surface normal, and correlated electrons with $\sigma_3 = \pm$ and $\sigma_4 = \pm$ go out at polar angles $\vartheta_3 = \vartheta_4 = 50^\circ$ and azimuthal angles $\varphi_3 = 0^\circ$ and $\varphi_4 = 180^\circ$. The symbols Σ_i^+ and Σ_i^- (with $i = 1,3$) in the LDOS panels stand for valence electron symmetry type Σ_i and spin $\pm$. In the pair emission intensity panels, the labels "all SOC", "$|2\rangle$ SOC", and "no SOC" indicate that the spectra were calculated with SOC in all four one-electron states, only in the valence state $|2\rangle$, and in none of the states, respectively. For clean W(110) we show in column A the valence electron LDOS $N_m^{\sigma_2}(E_2)$ with spin $\sigma_2 = +$ and the $(e,2e)$ intensities $I_{\sigma_3\sigma_4}^{\sigma_1}(E_2)$ associated with it. [For $\sigma_2 = -$ the LDOS results are the same, and so are the $(e,2e)$ intensities with all spin labels reversed.] For the magnetic system 1 ML Co on W(110), $N_m^{\sigma_2\mu}(E_2)$ and $I_{\sigma_3\sigma_4}^{\sigma_1\mu}(E_2)$ are shown in column B [only for $\mu = +$, since the results for $\mu = -$ are related to them by Eqs. (18) and (15)]. The left-hand (right-hand) panels pertain to valence electron spin $\sigma_2 = +$ $(-)$. In the LDOS panels Co1, W1, W2, and Wb refer to the Co adlayer, topmost, second, and bulk layer of W, respectively.

whereas they appear in the case of a reflecting step barrier, with their energy depending sensitively on the distance of the step barrier from the internuclear plane of the Co layer.

Including SOC, pronounced qualitative changes are seen in the Σ_3 LDOS. For spin up [Fig. 2(B), panel (a)] it reflects the Σ_1 peak around -0.9 eV for Co and W layers. For spin down [Fig. 2(B), panel (h)] the Co and adjacent W Σ_3 LDOS mirror the Σ_1 peak around 0 eV (Fermi energy) and exhibit a sharp feature at -0.7 eV.

We now turn to the pair emission intensities $I^{\sigma_1\mu}_{\sigma_3\sigma_4}(E_2)$ for $k_{2x} = 0$. Since according to Eq. (15) the intensities for minority spin index $\mu = -$ are then the same as those for $\mu = +$ with all the electron spins reversed, it suffices to show only $I^{\sigma_1+}_{\sigma_3\sigma_4}$. Let us first consider the parallel-spin intensities I^{++}_{++}, which according to the selection rules originate only from valence state spatial parts with symmetry Σ_3. Without SOC in all states [Fig. 2(B), panel (e)], there are two broad peaks, which correspond to the Σ_3 LDOS without SOC [panel (f)]. If SOC is switched on in the valence state [panel (d)], a third peak appears around -1 eV, which is due to the SOC-induced Σ_3 LDOS in Fig. 2(B), panel (a). Including SOC also in the LEED-type states leads to comparatively small changes [panel (c)]. In the parallel-spin intensities I^{-+}_{--}, there is also a prominent peak [around -1.1 eV in panels (j) and (k)], which owes its existence to SOC in the valence state. The intensities I^{-+}_{+-} and I^{-+}_{-+} with antiparallel spins of the two outgoing electrons are, for no SOC at all, equal and dominated by a peak around -0.8 eV [Fig. 2(B), panel (e)], which corresponds to the Σ_1 LDOS feature in panel (g). SOC causes these two intensities to differ substantially from each other, as is emphasized by the green (gray) area in Fig. 2(B), panels (c) and (d). The same holds for the antiparallel-spin intensities I^{++}_{+-} and I^{++}_{-+} [panels (j), (k), and (l)].

Comparing in Fig. 2 the heights of peaks of the $(e,2e)$ spectra for Co/W(110) with those for clean W(110), it is seen that the former are by a factor between 5 and 10 smaller than the latter. We ascribe this to the fact that W—with its much larger atomic number—produces much stronger elastic scattering amplitudes than Co. Since there are three LEED-type states in the $(e,2e)$ matrix elements, this effect is, loosely speaking, enhanced to the third power in $(e,2e)$.

For 2 ML Co on W(110), $(e,2e)$ intensities $I^{\sigma_1+}_{\sigma_3\sigma_4}(E_2)$—calculated with SOC in all states—and the associated LDOS at the surface Brillouin zone center are shown in Fig. 3. For spin up, the LDOS in the Co layer adjacent to the substrate [labeled Co1 in Figs. 3(a) and 3(b)] closely resembles that of 1 ML Co on W(110). The LDOS of the topmost Co layer (labeled Co2) is similar except for the absence of the peak at -0.9 eV, which we ascribed above to interference with backscattering from the substrate. In line with selection rules, the parallel-spin $(e,2e)$ intensities I^{++}_{++} and I^{-+}_{--} exhibit peaks at energies of maximal Σ_3 LDOS (below E_F). The relative difference between the direct and exchange antiparallel-spin intensities [marked in Figs. 3(c) and 3(f) by the green (gray) shading], which is a hallmark of SOC, is less than for 1 ML Co on W(110), but still sizable.

Comparing the heights of $(e,2e)$ peaks in Fig. 3 with those for 1 ML Co on W(110) [Fig. 2(B)], they are seen to be smaller. This is plausible since, first, as mentioned above, W is a much stronger scatterer than Co, and second, most of the $(e,2e)$ intensity comes from the topmost two layers, which now both consist of Co.

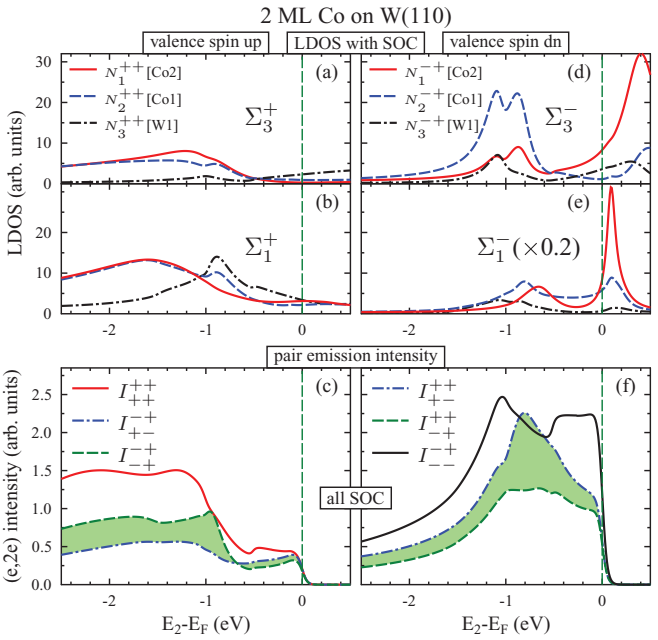

FIG. 3. (Color online) LDOS and $(e,2e)$ intensities for 2 ML Co on W(110). The layout and the notations used are analogous to those for 1 ML Co in Fig. 2, except that we now show only the results with SOC in all the four one-electron states. In the LDOS panels, the labels W1, Co1, and Co2 refer to the topmost W layer, the adjacent Co layer, and the topmost Co layer, respectively.

We now turn to the special case that the valence electron energy E_2 is kept constant and spectra are obtained as functions of the valence electron parallel-momentum component k_{2x}. As a representative value of E_2, we have chosen $E_F - 0.25$ eV. Regarding the LDOS, we recall the selection rule that only spatial parts of even symmetry with respect to the reaction plane (x,z) can contribute to the $(e,2e)$ matrix elements.

First, we address results for clean W(110) shown in column A of Fig. 4. Without SOC, the spin-up LDOS $N^+_m(k_{2x})$ is equal to the spin-down LDOS $N^-_m(k_{2x})$ and mirror symmetric with respect to $k_{2x} = 0$ [see panel (e)]. With SOC, this still holds for the bulk LDOS [see panel (a)]. For the near-surface layers, however, $N^+_m(k_{2x})$ [shown in panel (a) for $m = 1$ and 2, i.e., the first and second layer] is strongly asymmetric. So is $N^-_m(k_{2x})$, which is its mirror image, i.e., $N^-_m(k_{2x}) = N^+_m(-k_{2x})$. By virtue of this relation it is obvious from panel (a) of Fig. 4(A) that there is a substantial spin difference $N^+_m(k_{2x}) - N^-_m(k_{2x})$.

The $(e,2e)$ intensities I^+_{++}, I^-_{+-}, and I^-_{-+}, which originate from spin-up valence electrons, are shown in Fig. 4(A), panels (b), (c), and (d). Those from spin-down valence electrons are obtained from them by virtue of the relation [cf. Eq. (15)] $I^{-\sigma_1}_{-\sigma_3-\sigma_4}(k_{2x}) = I^{\sigma_1}_{\sigma_3,\sigma_4}(-k_{2x})$. The spectra obtained without any SOC [panel (d)] are seen to be symmetric, in line with the symmetry of the corresponding LDOS. This symmetry is already broken by including SOC only in the valence state [panel (c)] and even more so if SOC is present in all states [panel (b)].

For the ferromagnetic system 1 ML Co on W(110), results for spin-up and spin-down valence electrons are of course

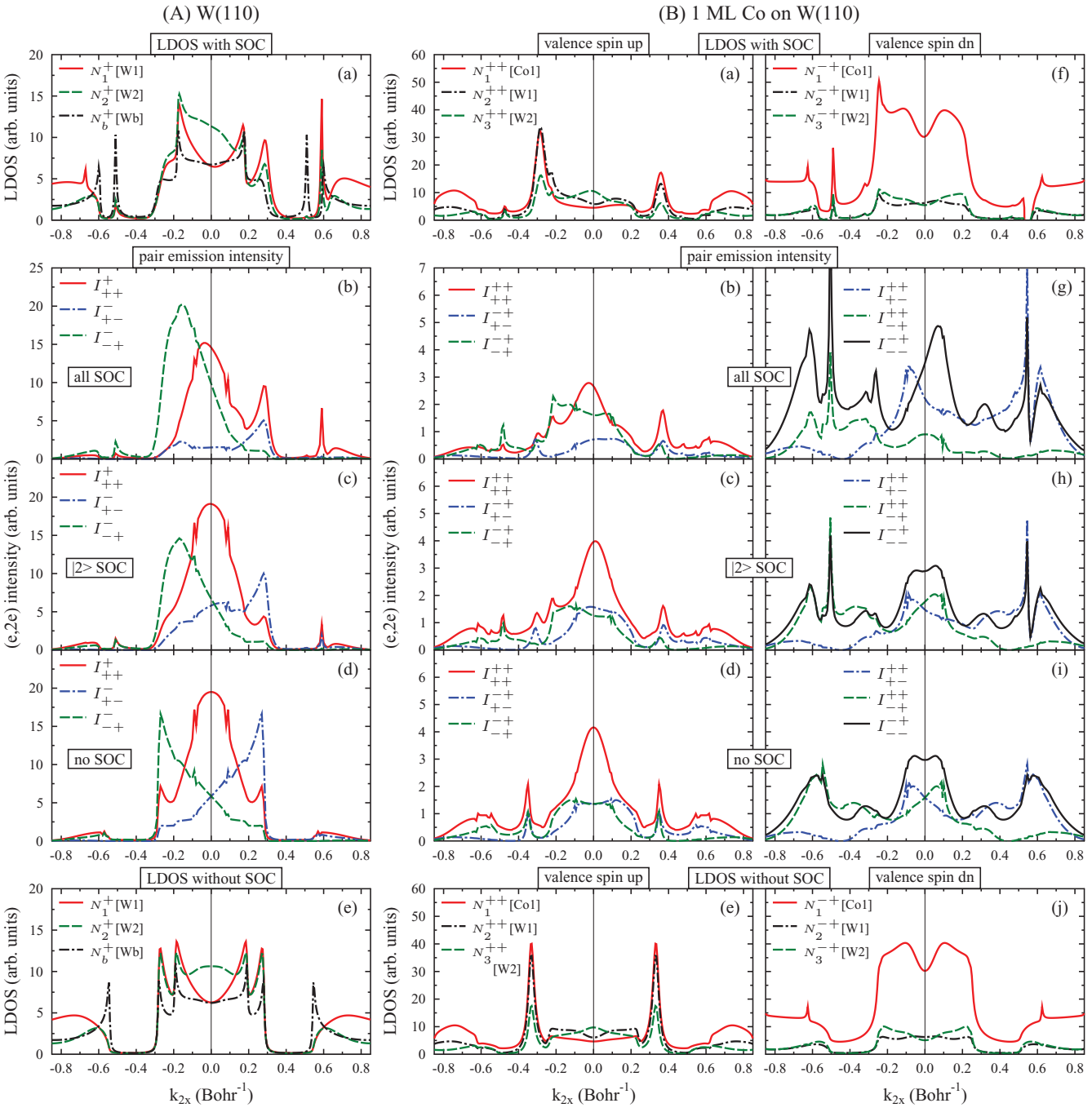

FIG. 4. (Color online) Spin-resolved valence electron densities of even (with respect to the xz plane) states $N_m^{\sigma_2}(E_2,k_{2x},k_{2y}=0)$ for fixed energy $E_2 = E_F - 0.25$ eV as functions of the valence electron surface-parallel momentum component k_{2x} and corresponding $(e,2e)$ intensities [cf. Eq. (7)] for normally incident primary electrons with energy 27 eV and spin $\sigma_1 = \pm$. For clean W(110) we show in column A the valence electron LDOS $N_m^{\sigma_2}(k_{2x})$ with spin $\sigma_2 = +$ and the $(e,2e)$ intensities $I_{\sigma_3\sigma_4}^{\sigma_1}(k_{2x})$ associated with it. [For $\sigma_2 = -$, the LDOS is—according to Eq. (18)—the mirror image of the $\sigma_2 = +$ case and so are the $(e,2e)$ intensities with all spin labels reversed.] For the magnetic system 1 ML Co on W(110), $N_m^{\sigma_2\mu}(k_{2x})$ and $I_{\sigma_3\sigma_4}^{\sigma_1\mu}(k_{2x})$ are shown in column B [only for $\mu = +$, since the results for $\mu = -$ are related to them by Eqs. (18) and (15)]. The left-hand (right-hand) panels pertain to valence electron spin $\sigma_2 = +\,(-)$. In the $(e,2e)$ panels, the labels "all SOC", "$|2\rangle$ SOC," and "no SOC" indicate that the spectra were calculated with SOC in all four one-electron states, only in the valence state $|2\rangle$, and in none of the states, respectively. In the LDOS panels Co1, W1, W2, and Wb refer to the Co adlayer, topmost, second, and bulk layer of W, respectively.

different, and both are therefore shown, in column B of Fig. 4. Without SOC, the LDOS [panels (e) and (j)] is symmetric. For spin up, it is dominated by two peaks, at ± 0.33 Bohr^{-1}, which have the most weight in the Co layer and in the adjacent W layer. With SOC, the LDOS becomes asymmetric to a similar degree as in the case of clean W(110). This is most noteworthy for the Co layer, in which SOC is much weaker than in W.

Turning to the $(e,2e)$ intensities $I^{\sigma_1\mu}_{\sigma_3\sigma_4}(k_{2x})$ for 1 ML Co on W(110), we recall that according to Eq. (15) the intensities for $\mu = -$ are obtainable from those for $\mu = +$. We therefore show only the latter [in Fig. 4(B)]. In much the same way as for clean W(110), the symmetry of the no-SOC spectra is seen to be broken by including SOC in the valence state and furthermore in all states.

Since the resolution of the spins of the two emitted electrons is to date not feasible experimentally, it is of particular interest to consider the spin-summed intensities $I^{\sigma_1\mu}(k_{2x})$ [cf. Eq. (10)]. Because of the relation $I^{\sigma_1-}(k_{2x}) = I^{-\sigma_1+}(-k_{2x})$ [cf. Eq. (15)] it suffices to show only $I^{\sigma_1+}(k_{2x})$ with $\sigma_1 = \pm$ [see Figs. 5(a)–5(c)]. Without SOC, all the curves would be mirror symmetric, i.e., $I^{\sigma_1}(k_{2x}) = I^{\sigma_1}(-k_{2x})$. The absence of this mirror symmetry in the intensities in Fig. 5, which were calculated fully relativistically, is therefore a manifestation of SOC. While strongest for clean W(110), it is still fairly big for 1 ML Co on W(110) and clearly visible for 2 ML Co on W(110).

To separate, for the magnetic systems, the effects of exchange interaction and SOC, and to compare the latter with the SOC effect for clean W(110), we show [in panels (d)–(f) of Fig. 5] the exchange and spin-orbit asymmetries $A_{\rm ex}$ and $A_{\rm so}$ plus the magnetic dichroic asymmetry A_u, which are obtained from the intensities according to Eqs. (11b)–(11d). As derived analytically in Sec. III [cf. Eqs. (17a)–(17c)], $A_{\rm so}$ and A_u are indeed antisymmetric, whereas $A_{\rm ex}$ is symmetric. $A_{\rm so}$ is seen to be strongest for clean W (with peak heights up to about 70%). For 1 ML Co, it still reaches about 30%, and for 2 ML Co on W(110) about 20%. We note that the latter values are much larger than typical values which we obtained for a semi-infinite Co crystal surface. In the range $|k_{2x}| < 0.4$ Bohr^{-1}, A_u has similar magnitude as $A_{\rm so}$, whereas for $|k_{2x}| > 0.4$ Bohr^{-1} it exhibits several very narrow peaks of almost 50%. These originate from valence electron surface states as shown, for the case of 1 ML Co, in Fig. 4.

The asymmetries shown in Fig. 5 were calculated with SOC in all four one-electron states. In order to get more physical insight, we performed analogous calculations with SOC only in the valence state, SOC only in the primary and outgoing electron states, and with no SOC at all. The results for clean W(110) and for 1 ML Co on W(110) are presented in Fig. 6 (only for $k_{2x} \geqslant 0$ because of the mirror symmetry or antisymmmetry as seen in Fig. 5). For clean W(110), panels (a), (b), and (c) of Fig. 6 reveal that $A_{\rm so}$ is largely determined by SOC in the LEED-type states $|1\rangle$, $|3\rangle$, and $|4\rangle$, whereas SOC in the valence state $|2\rangle$ has an appreciable influence only for small k_{2x} below about 0.4 Bohr^{-1} and near 0.6 Bohr^{-1}. For 1 ML Co on W(110) panels (e), (f), and (g) support a similar conclusion for $A_{\rm so}$, with SOC in state $|2\rangle$ playing an even minor role. $A_{\rm ex}$ with SOC in all states differs strongly from the $A_{\rm ex}$ calculated with no SOC [panel (h)] and with SOC only in the valence state [panel (f)]. Like $A_{\rm so}$ it is mainly shaped by SOC in the LEED states.

The opposite holds for the dichroic asymmetry A_u. The curve obtained with SOC in all states [Fig. 6(e)] is very similar to the one with SOC only in the valence state $|2\rangle$ [Fig. 6(f)]. This appears plausible for the following reason. The left-right asymmetries, which are produced by SOC in each of the LEED-type states, are approximately averaged

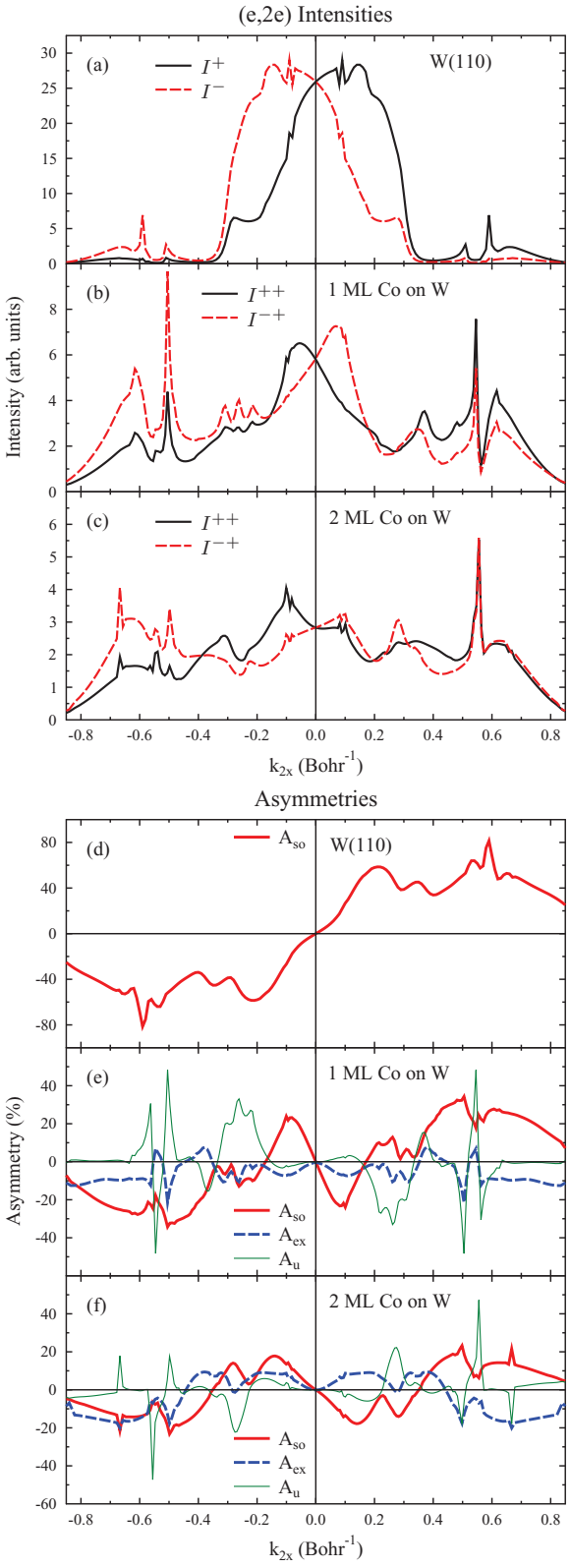

FIG. 5. (Color online) Panels (a), (b), and (c) display the spin-summed $(e,2e)$ intensities $I^{\sigma_1}(k_{2x})$ for clean W(110) and $I^{\sigma_1+}(k_{2x})$ for Co on W [cf. Eq. (10)] with primary spin $\sigma_1 = \pm$. The fixed primary and valence electron energies are 27 eV and $E_F - 0.25$ eV. The corresponding spin-orbit and exchange asymmetries $A_{\rm so}$ and $A_{\rm ex}$ as well as the dichroic asymmetry A_u [cf. Eqs. (11b), (11c), and (11d)] are shown in panels (d), (e), and (f).

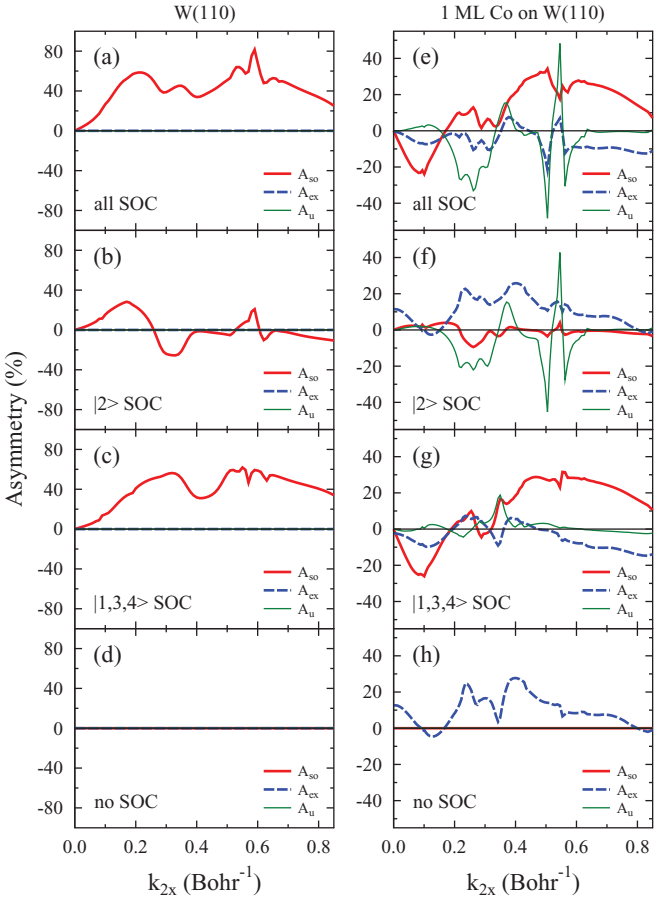

FIG. 6. (Color online) For clean W(110) and for 1 ML Co on W(110), the three asymmetries A_{so}, A_{ex}, and A_u [cf. Eqs. (11b), (11c), and (11d)], which were shown in Figs. 5(d) and 5(e), are displayed with SOC selectively present only in some of the one-electron states. In the individual panels, the labels "all SOC", "$|2\rangle$ SOC", "$|1,3,4\rangle$ SOC", and "no SOC" indicate that the asymmetries were obtained with SOC in all four one-electron states, only in the valence state $|2\rangle$, only in the primary state $|1\rangle$ and in the outgoing electron states $|3,4\rangle$, and in none of the states, respectively. Note that the curves are shown only in the momentum range from 0 to 0.85 Bohr^{-1}, since in the range from -0.85 to 0 Bohr^{-1} they are equivalent by symmetry (as shown explicitly in Fig. 5).

out, since A_u involves a sum over the primary electron spin [cf. Eq. (11d)] together with the sum over the spins of the two outgoing electrons [cf. Eq. (10)]. Therefore, there remains mainly SOC in $|2\rangle$ to produce A_u.

The above properties of the three asymmetries, which were gleaned from Fig. 6 for the fixed valence electron energy $E_F - 0.25$ eV, are corroborated by the results of analogous calculations for other valence energies and for 2 ML Co on W(110).

The theoretical $(e,2e)$ intensities and asymmetries as functions of the valence electron momentum component k_{2x} shown in Fig. 5 were obtained for fixed valence electron energy E_2 (as determined by energy conservation) and fixed emission angles $\vartheta_3 = \vartheta_4 = 50^\circ$ and $\varphi_3 = 0^\circ$ and $\varphi_4 = 180^\circ$. In view of making contact with the experimental asymmetries published by Samarin *et al.*,[22] we have to note that the latter were obtained for valence electron energies E_2 within a 0.5 eV band just below the Fermi energy and for a range of emission angles, which correspond to the acceptance angles of the two position-sensitive detectors (cf. Ref. 22). Furthermore, there may be some divergence of the primary electron beam around its nominal direction of incidence.

To take care of these experimental conditions, we adopted the following statistical approach. For a given primary beam energy E_1 and each fixed k_{2x}, a large number of sets $(E_2,\vartheta_3,\vartheta_4,\varphi_3,\varphi_4,\vartheta_1,\varphi_1)$ is randomly generated subject to the conditions that (1) the valence electron energy E_2 lies within the range chosen in the experiment, (2) the emission directions are within the acceptance angles of the detectors, and (3) the primary beam has a specified cone of divergence around the surface normal. According to conservation of energy and surface-parallel momentum [cf. Eqs. (8) and (9)] each of these sets is equivalent to a set $(E_3,E_4,\vec{k}_3^{\parallel},\vec{k}_4^{\parallel},\vec{k}_1^{\parallel})$. For each of the latter sets, the $(e,2e)$ intensities $I^{\sigma_1\mu}(E_3,E_4,\vec{k}_3^{\parallel},\vec{k}_4^{\parallel},\vec{k}_1^{\parallel})$ are calculated, and then averaged over the sets to yield the k_{2x} intensity distributions $I^{\sigma_1\mu}(k_{2x})$. As appropriate for the experiment,[22] we chose the opening angle of the acceptance cone for the detected electrons as 20°, the primary beam divergence as 2°, and the valence energy interval $[E_F - 0.5\,\text{eV}, E_F]$. In addition, we performed calculations for the interval $[E_F - 1.0\,\text{eV}, E_F - 0.5\,\text{eV}]$.

For a valid comparison with experimental data, it is furthermore pertinent to address the following issue. While our theoretical $(e,2e)$ intensities only involve electron pairs produced in a single collision process between the primary electron and a valence electron, experimental data may in addition comprise electron pairs, which originate from multiple collision processes. Since for the latter pairs the energy and momentum conservation [Eqs. (8) and (9)] does not hold, the $(e,2e)$ intensities can no longer be represented as functions of the valence electron energy E_2 and momentum component k_{2x} [cf. Eq. (15)] and be related to the valence electron densities of states. More generally, these pairs degrade the physical information content of $(e,2e)$. It is therefore important to ensure that they are far outnumbered by the pairs from single collisions. For a given primary energy E_1, this can be achieved by choosing the total energy $E_{\text{sum}} = E_3 + E_4$ of the detected pair within a suitable range. Since the maximal valence electron energy (with respect to the vacuum level) is $E_2^{\max} = -\Phi = E_F$, where Φ is the work function and E_F the Fermi energy, energy conservation [cf. Eq. (8)] implies that the maximal total energy is $E_{\text{sum}}^{\max} = E_1 + E_F$. Electron pairs with $E_{\text{sum}}^{\max}$ can only originate from a single collision of the primary electron with an electron at the Fermi energy E_F, since additional collision events entail energy losses and the emitted pair has $E_{\text{sum}} < E_{\text{sum}}^{\max}$. Pairs with $E_{\text{sum}} = E_{\text{sum}}^{\max} - \Delta E$ can stem from a single collision with a valence electron with energy $E_F - \Delta E$ or from a multiple collision process with an energy loss between 0 and ΔE. It is therefore clear that the number of pairs from multiple collisions increases with increasing ΔE. An estimate of the ratio of these undesirable pairs to those from single collisions has been obtained experimentally by Samarin *et al.*[52] for the W(001) surface: for ΔE up to a few eV, i.e., for E_{sum} up to a few eV below $E_{\text{sum}}^{\max}$, pairs generated by single collisions predominate. This finding was corroborated by a good overall agreement between experimental $(e,2e)$ data and their theoretical counterparts.[53]

With regard to the single collisions, we would like to recall an essential aspect. After the collision, the two electrons move mainly in the forward direction. One might therefore expect most of them to disappear into the crystal. Elastic reflection at atomic layers inside the crystal however can redirect the primary electron before the collision or the two electrons after the collision towards the surface and thus allow the two electrons to reach the detectors. The vital importance of elastic reflection for low energy $(e,2e)$ from surfaces has been demonstrated by numerical calculations in Ref. 53 (see in particular Fig. 5), where also references to further evidence are given.

A final point to be taken into account is inherent in the experimental coincidence technique used by Samarin *et al.*[22] In addition to the true pair emission events, which involve a collision, there is an additional contribution to the measured intensities, which arises from so-called "spurious coincidence events": two primary electrons leave the electron gun within the time interval; each of them is inelastically backscattered from the surface, and one is detected in one detector, the other in the other detector. Thus there are actually two single events instead of a genuine pair event. According to Ref. 54, this contribution amounts to about 10% of the peak intensities and is hardly spin dependent. To make more appropriate contact with the experimental data, we therefore augmented our calculated pair emission intensities by a spin-independent constant value taken as 10% of the main peak heights. From these augmented intensities, asymmetry distributions $A_{\rm so}(k_{2x})$ and $A_{\rm ex}(k_{2x})$ were then obtained according to Eqs. (11b) and (11c).

These results are presented in Fig. 7 together with the experimental data from Ref. 22. For Co on W(110), it must be noted that the theoretical asymmetries are those for two pseudomorphic monolayers, whereas the experimental asymmetries were obtained for an incommensurate hcp-like Co film of nominally three monolayers. Given this difference, the agreement between theoretical and experimental exchange asymmetry $A_{\rm ex}$ in Fig. 7(c) is rather good in the momentum range from -0.4 to $+0.4$. In this range, the calculated and measured spin-orbit asymmetries for both Co on W(110) and for clean W(110) agree similarly well, with the theoretical extrema for W(110) exceeding the experimental ones by a factor of about 1.5. Comparing $A_{\rm so}$ for clean W and Co on W, experiment and theory have two results in common. First, around -0.2 $(+0.2)$ there is a minimum (maximum) for clean W and a maximum (minimum) for Co on W. Second, the magnitude of these extrema is much smaller for Co on W, but still appreciable, and much larger than what one would obtain from a semi-infinite Co crystal. For momentum values outside the range $[-0.4,0.4]$, the agreement is less satisfactory. As a possible reason, we propose the following. The difference in the energies of the two emitted electrons, which is zero for $k_{2x}=0$, increases with increasing k_{2x}. For larger k_{2x}, one of the electrons has a rather high energy and the other a rather low one. Since the state of the electron with the very low energy is more sensitive to variations of the surface barrier in theory and to contaminations of the surface in experiment, discrepancies between theory and experiment can arise more readily.

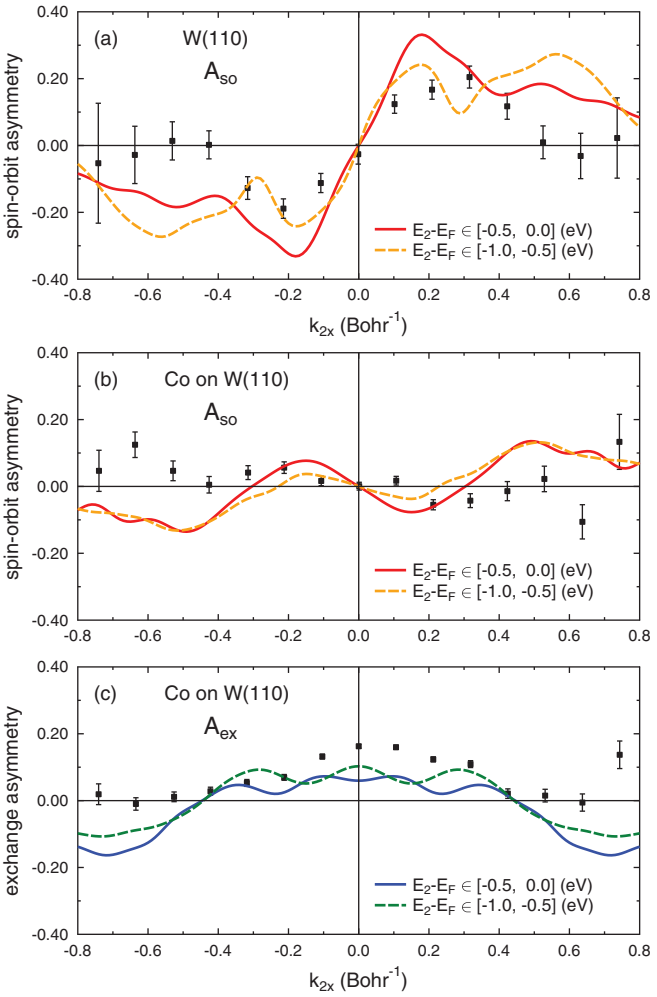

FIG. 7. (Color online) Comparison of theoretical $(e,2e)$ asymmetries (solid and dashed lines) with experimental ones[22] (dots with error bars) as functions of the valence electron surface-parallel momentum k_{2x}. The primary electron energy is 27 eV. The experimental valence electron energies range from $E_F-0.5$ eV to E_F. Theoretical results are shown for this range (solid lines) and for the range from $E_F-1.0$ eV to $E_F-0.5$ eV (dashed lines). (a) $A_{\rm so}$ for clean W(110); (b) and (c): $A_{\rm so}$ and $A_{\rm ex}$ for Co on W(110); the theoretical curves were calculated for two pseudomorphic Co monolayers on W(110), whereas the experimental data were obtained for a noncommensurate hcp-like Co film of nominally three layers. The asymmetries shown in Ref. 22 are the raw ones as measured for a primary beam polarization of 66%.[54] For comparison with theory, we normalized them to 100% polarization, i.e., divided the raw ones by 0.66.

V. CONCLUSION

Spin-orbit coupling (SOC) plays an important role in low energy $(e,2e)$ from ferromagnetic surface systems, which involve a large-Z material. We presented an $(e,2e)$ theory for such systems, which includes SOC and magnetic exchange on an equal footing on the basis of a Dirac equation with an effective magnetic field and incorporates the correlation between the two emitted electrons.

After deriving, for cubic(110) surfaces, general symmetry properties of the observable fully spin-resolved intensities

and asymmetries, we proceeded to applying our formalism to ferromagnetic ultrathin films of 1 and 2 ML Co on W(110). As a prerequisite, we performed *ab initio* ground state calculations in the framework of density functional theory, which yielded the layer-dependent magnetic moments and provided the real part of the quasiparticle potentials, which were used in the subsequent $(e,2e)$ calculations.

Fully spin-resolved $(e,2e)$ intensities were presented as functions of the energy and surface-parallel momentum of the relevant valence electron. This facilitated an analysis of the $(e,2e)$ spectra in terms of the simultaneously calculated spin- and layer-resolved valence electron densities of states. In experimental reality, SOC acts in the three LEED-type states as well as in the valence state and observable SOC effects result from a combination of the SOC-induced properties of these individual states. For finding out which states might predominantly be responsible for an observed SOC effect, theory has the advantage of being able to selectively switch off SOC in the individual one-electron states. By comparing the results of such "switch-off"calculations with those of an "all SOC"calculation, we could identify SOC in the valence state or in the LEED-type states as the origin of specific SOC-induced $(e,2e)$ features.

In particular, we analyzed in this way three asymmetries derived from the spin-dependent $(e,2e)$ intensities from 1 ML and 2 ML of Co on W(110). The SOC-induced A_{so} as a function of the valence electron momentum turned out to be mainly determined by SOC in the LEED-type states. A_{ex}, which requires magnetic exchange for its existence, was found to be very strongly affected in magnitude and shape by SOC in the LEED states. Since our calculated A_{so} and A_{ex} encouragingly agree with their experimental counterparts,[22] our findings are likely to apply to them as well.

In contrast to A_{so} and to A_{ex}, the dichroic asymmetry A_u originates essentially from SOC in the valence state of Co on W(110). This recommends it as potentially useful for studying SOC in the occupied states of ultrathin magnetic films on large-Z nonmagnetic substrates. According to the original definition of A_u [Eq. (11d)], its measurement requires a reversal of the magnetization. To obtain $A_u(k_{2x})$ for constant valence energy E_2, an experimentally easier and perhaps more reliable way is however offered by a symmetry relation between the underlying spin-dependent intensities [cf. Eq. (16)]. By virtue of the energy and momentum conservation conditions this simply requires an interchange of the two emitted-electron energies at the detectors.

ACKNOWLEDGMENTS

We would like to thank S. Samarin and F. O. Schumann for helpful discussions and information on experimental data.

[1] D. Sander, J. Phys.: Condens. Matter **16**, R603 (2004).
[2] *Spin-Orbit-Induced Spectroscopies of Magnetic Solids*, edited by H. Ebert and G. Schuetz, Lecture Notes in Physics, Vol. 466 (Springer, Berlin, 1996).
[3] S. F. Alvarado, R. Feder, H. Hopster, F. Ciccacci, and H. Pleyer, Z. Phys. B **49**, 129 (1982).
[4] E. Tamura, B. Ackermann, and R. Feder, J. Phys. C **17**, 5455 (1984).
[5] *Polarized Electrons in Surface Physics*, edited by R. Feder (World Scientific, Singapore, 1985), Chap. 4.
[6] W. Kuch and C. M. Schneider, Rep. Prog. Phys. **64**, 147 (2001).
[7] J. Henk and A. Ernst, J. Electron Spectrosc. Relat. Phenom. **125**, 107 (2002).
[8] C. E. Violbarbosa, S. Quardi, G. H. Fecher, D. Ebke, and C. Felser [J. Electron Spectrosc. Relat. Phenom. (to be published)].
[9] A. Dorn, A. Elliott, J. Lower, E. Weigold, J. Berakdar, A. Engelns, and H. Klar, Phys. Rev. Lett. **80**, 257 (1998).
[10] R. Hubele, A. LaForge, M. Schulz *et al.*, Phys. Rev. Lett. **110**, 133201 (2013).
[11] J. Ullrich, R. Moshammer, A. Dorn, R. Dörner, L. Ph.H. Schmidt, and H. Schmidt-Böcking, Rep. Prog. Phys. **66**, 1463 (2003).
[12] L. Avaldi and A. Huetz, J. Phys. B **38**, S861 (2005).
[13] A. Knapp, A. Kheifets, I. Bray, Th. Weber, A. L. Landers, S. Schössler, T. Jahnke, J. Nickles, S. Kammer, O. Jagutzki, L. Ph. H. Schmidt, M. Schöffler, T. Osipov, M. H. Prior, H. Schmidt-Böcking, C. L. Cocke, and R. Dörner, J. Phys. B **38**, 615 (2005).
[14] R. Feder and H. Gollisch, in *Solid State Photoemission and Related Methods*, edited by W. Schattke and M. A. Van Hove (Wiley-VCH, Weinheim, 2003).
[15] F. Giebels, H. Gollisch, R. Feder, F. O. Schumann, C. Winkler, and J. Kirschner, Phys. Rev. B **84**, 165421 (2011).
[16] S. Samarin, O. M. Artamonov, V. N. Petrov, M. Kostylev, L. Pravica, A. Baraban, and J. F. Williams, Phys. Rev. B **84**, 184433 (2011).
[17] Z. Wei, F. O. Schumann, R. S. Dhaka, and J. Kirschner, Phys. Rev. B **85**, 195120 (2012).
[18] F. Giebels, H. Gollisch, and R. Feder, Phys. Rev. B **87**, 035124 (2013).
[19] H. Gollisch, X. Yi, T. Scheunemann, and R. Feder, J. Phys.: Condens. Matter **11**, 9555 (1999).
[20] S. Samarin, O. M. Artamonov, A. D. Sergeant, J. Kirschner, A. Morozov, and J. F. Williams, Phys. Rev. B **70**, 073403 (2004).
[21] S. Samarin, O. M. Artamonov, A. D. Sergeant, and J. F. Williams, Phys. Rev. B **72**, 235419 (2005).
[22] S. Samarin, O. M. Artamonov, A. D. Sergeant, R. Stamps, and J. F. Williams, Phys. Rev. Lett. **97**, 096402 (2006).
[23] S. Samarin, O. M. Artamonov, A. D. Sergeant, and J. F. Williams, Surf. Sci. **601**, 4343 (2007).
[24] S. Samarin, O. M. Artamonov, A. D. Sergeant, J. Kirschner, and J. F. Williams, J. Phys.: Conf. Ser. **100**, 072033 (2008).
[25] E. Engel and R. M. Dreizler, *Density Functional Theory* (Springer, Berlin-Heidelberg, 2011).
[26] S. V. Halilov, E. Tamura, D. Meinert, H. Gollisch, and R. Feder, J. Phys.: Condens. Matter **5**, 3859 (1993).
[27] H. Gollisch, N. v. Schwartzenberg, and R. Feder, Phys. Rev. B **74**, 075407 (2006).
[28] T. Inui, Y. Tanabe, and Y. Onodera, *Group Theory and Its Applications in Physics*, 1st ed., Springer Series in Solid State Sciences Vol. 78 (Springer, Berlin, 1990).

[29]M. Arnold, G. Hupfauer, P. Bayer, L. Hammer, K. Heinz, B. Kohler, and M. Scheffler, Surf. Sci. **382**, 288 (1997).
[30]G. Teeter, J. L. Erskine, F. Shi, and M. A. Van Hove, Phys. Rev. B **60**, 1975 (1999).
[31]D. Venus, S. Cool, and M. Plihal, Surf. Sci. **446**, 199 (2000).
[32]H. L. Meyerheim, D. Sander, R. Popescu, P. Steadman, S. Ferrer, and J. Kirschner, Surf. Sci. **475**, 103 (2001).
[33]H. Knoppe and E. Bauer, Phys. Rev. B **48**, 1794 (1993).
[34]E. Bauer, J. Phys.: Condens. Matter **11**, 9365 (1999).
[35]M. Pratzer, H. J. Elmers, and M. Getzlaff, Phys. Rev. B **67**, 153405 (2003).
[36]See www.flapw.de.
[37]X. Qian and W. Hubner, Phys. Rev. B **60**, 16192 (1999).
[38]I. Galanakis, M. Alouani, and H. Dreysse, Phys. Rev. B **62**, 3923 (2000).
[39]S. H. Vosko, L. Wilk, and M. Nusair, Can. J. Phys. **58**, 1200 (1980).
[40]S. N. Samarin, J. F. Williams, A. D. Sergeant, O. M. Artamonov, H. Gollisch, and R. Feder, Phys. Rev. B **76**, 125402 (2007).
[41]H. J. Herlt, R. Feder, G. Meister, and E. G. Bauer, Solid State Commun. **38**, 973 (1981).
[42]E. G. Bauer (private communication).
[43]J. Feydt, A. Elbe, H. Engelhard, G. Meister, Ch. Jung, and A. Goldmann, Phys. Rev. B **58**, 14007 (1998).
[44]K. Miyamoto, A. Kimura, K. Kuroda, T. Okuda, K. Shimada, H. Namatame, M. Taniguchi, and M. Donath, Phys. Rev. Lett. **108**, 066808 (2012).
[45]J. Sanchez-Barriga, J. Minar, J. Braun, A. Varykhalov, V. Boni, I. Di Marco, O. Rader, V. Bellini, F. Manghi, H. Ebert, M. I. Katsnelson, A. I. Lichtenstein, O. Eriksson, W. Eberhardt, H. A. Durr, and J. Fink, Phys. Rev. B **82**, 104414 (2010).
[46]D. P. Pappas, K. P. Kämper, B. P. Miller, H. Hopster, D. E. Fowler, C. R. Brundle, A. C. Luntz, and Z. X. Shen, Phys. Rev. Lett. **66**, 504 (1991).
[47]M. Getzlaff, J. Bansmann, and G. Schönhense, Solid State Commun. **87**, 467 (1993).
[48]F. Passek, M. Donath, and K. Ertl, J. Magn. Magn. Mater. **159**, 103 (1996).
[49]H. Gollisch and R. Feder, J. Phys.: Condens. Matter **16**, 2207 (2004).
[50]K. Miyamoto, A. Kimura, T. Okuda, K. Shimada, H. Iwasawa, H. Hayashi, H. Namatame, M. Taniguchi, and M. Donath, Phys. Rev. B **86**, 161411 (2012).
[51]H. Mirhosseini, M. Flieger, and J. Henk, New J. Phys. **15**, 033019 (2013).
[52]S. N. Samarin, O. M. Artamonov, H. Schwabe, and J. Kirschner, in *Coincidence Studies of Electron and Photon Impact Ionization*, edited by C. T. Whelan and H. R. J. Walters (Plenum Press, New York and London, 1997).
[53]R. Feder, H. Gollisch, D. Meinert, T. Scheunemann, O. M. Artamonov, S. N. Samarin, and J. Kirschner, Phys. Rev. B **58**, 16418 (1998).
[54]S. Samarin (private communication).